CERN-PBC-Notes-2023-006

25 February 2024

Conceptual Design of a Neutral Beam Line for Phase 2 of the HIKE Experiment

L. J. Nevay[1], M. Van Dijk, L. Gatignon[2], E. G. Parozzi, J. Bernhard.
CERN, CH-1211 Geneva, Switzerland

Keywords: `ECN3, HIKE, neutral beam, beam design`

Summary

This document describes the first design concept of a 120 m long beam line in the TCC8/ECN3 complex of the CERN North Area that is aimed at delivering a high-intensity, neutral kaon beam for the second phase of the proposed HIKE Experiment. The beam design has been developed in the framework of the PBC Conventional Beams Working Group and comprises of a target, magnetic sweeping; a proton dump; photon absorber; and a three stage collimation system. This report details the beamline design chosen based on the requirements to generate and select a beam of K_L^0. A discussion of beam content and experimental backgrounds is also presented.

[1]Corresponding author: laurie.nevay@cern.ch
[2]Currently at Physics Department, Lancaster University, Lancaster, United Kingdom, LA1 4YB

Contents

1 Introduction

For HIKE Phase 2, a beamline is envisioned to produce a beam of K_L^0 particles. The experiment will be a multi-purpose K_L^0 decay experiment to measure rare decay modes; in particular $K_L^0 \to \pi^0 l^+ l^-$ [1]. The beam concept is based on the design ideas of the neutral K_L^0 and K_S^0 beam for the NA48 experiment [2].

The K_L^0 particles would be produced in a foreseen new graphite target in the T10 target station. The beam would collide with the target at an angle of 2.4 mrad to increase the ratio of K_L^0 to other backgrounds with some tolerance in this value should it be desired to adjust it in future. The beamline should therefore remove all other particles as well as is reasonably possible. Given the desired neutral beam, charged particles can be removed via magnetic fields. The beamline should define an acceptance cone of 0.4 mrad, as requested by HIKE Phase 2, and clean particles outside this cone. Any charged secondaries generated by collimating elements should also be removed from the experimental acceptance, and the regeneration of K_S^0 should be minimised where possible, particularly late in the beam line. If these conditions are met, then the main experimental backgrounds will be the Greenlee modes $K_L^0 \to \gamma\gamma l^+ l^-$ of the respective decays [3] that can not be reduced by the beamline. Decays of K_L^0 themselves as well as Λ^0 will be also a source of background charged particles.

The beamline design is based on experience with the K_L^0 beamlines for NA31 and NA48 [4] and it should be ideally synertistic with the HIKE Phase 1 experiment to minimise cost with, also ideally, no major civil engineering works. A length of 120 m was chosen to ensure the K_S^0 content has sufficiently decayed and whilst it is 18 m longer than the Phase 1 beamline, it is compatible with the detector installation remaining in place as magnets from Phase 1 will be removed. As the desired K_L^0 particle is neutral, no magnetic chicane can be used to select a desired momentum, and a broad, continuous spectrum will be transmitted.

1.1 Design Overview

The overall beamline design is shown in Figure 1. From the beginning of the line (*left*), the target is housed in a shielding complex, with the $S = 0$ point of the beamline defined as the centre of the target. The beam would impinge on the target at a 2.4 mrad downward (vertical) angle passing through this zero point at the centre. A range of angles could be used in principle, but for this report, only this baseline value of 2.4 mrad has been considered. After the target, a vertical dipole magnet is used to immediately deflect the remaining protons downwards into a proton dump. After the proton dump, a horizontal dipole magnet is used to sweep away any charged particles emerging. The existing HIKE Phase 1 TAX is not required but it can remain in place provided it is not a limiting aperture for the acceptance cone of the beam. Aside from the target, the TAX is the only part of the beamline in air. Two collimation stations follow this, each with an iron shield in front of them to prevent any possible backgrounds passing around the side of the collimator. The first collimator defines the beam to be a cone with an opening angle of 0.4 mrad relative to the central axis of the target and the beamline. The second cleaning collimator cleans any undesired components created or scattered in the defining collimator. Dipole magnets after each collimator are used to sweep any charged particle background created in the collimators. Finally, a wider aperture active collimator meets the experiment at a distance of 120 m from the centre of

the target. A detailed list of components is given in Appendix A.

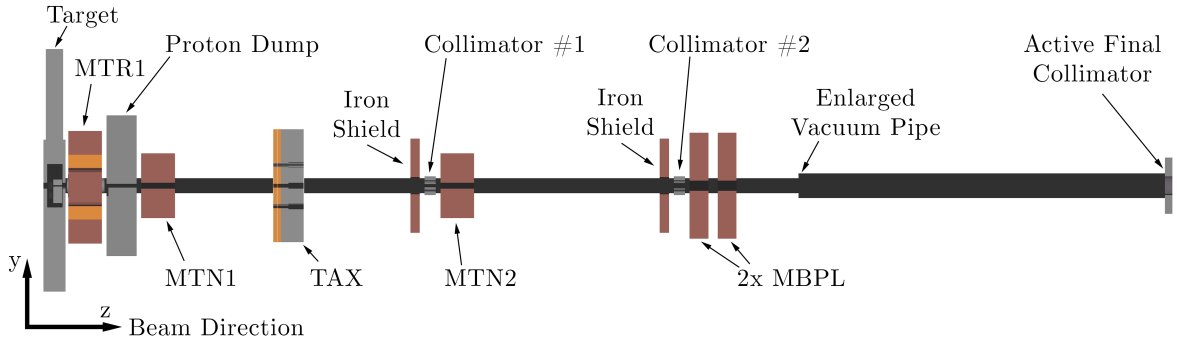

Figure 1: Overview of complete beamline with the beam travelling from left to right. The view has the horizontal (z) scale compressed by a factor of 10 with respect to the vertical (y) scale.

In this report, the handling of the proton beam is first discussed in Section 2, followed by the collimation system in Section 3. A gamma converter and the vacuum system are described in Sections 4 and 5 respectively. Shielding is discussed in Section 6, before the expected beam composition and experimental backgrounds are described in Section 7.

2 Proton Beam Handling

The assumed spill intensity for this report is 2×10^{13} 400 GeV c^{-1} protons on target (p.o.t.) per 4.8 s spill from the SPS on the T10 target from the P42 beamline. The beam distribution at the centre of the target is described in Table 1.

Table 1: Proton beam parameters at the centre of the target ignoring particle-matter interactions.

Parameter	Value
σ_x	0.212 mm
σ_y	0.208 mm
σ'_x	0.062×10^{-3}
σ'_y	0.212×10^{-3}
θ_y	-2.4 mrad
θ_x	0 mrad

The ratio of secondary particles produced from the collisions depends on the angle selected with respect to the beam [1, 5]. In this setup, the beam would be collided at an angle to the target and the target–beamline–experiment section built in a straight line. The crossing angle affects the ratio of particle species and their spectra in the beamline and whilst 2.4 mrad is considered herein as the nominal value, the precise figure may be refined later. HIKE Phase 3 (formerly known as KLEVER) may require up to a 8 mrad crossing angle. The 2.4 mrad angle is chosen to be negative in the vertical direction so any additional secondary products generally point downwards into the ground.

2.1 Target

The length of the target is chosen to be one nuclear interaction length, which is the same as the current T10 target, and hence also the same number of nuclear interaction lengths as is for HIKE Phase 1. For the current T10 target, 40 cm of Beryllium is used. The new target material proposed is graphite due to better handling capabilities. With a density of $\rho = 2.210\,\mathrm{g\,cm^{-3}}$), one interaction length of graphite corresponds to 38.824 cm [6]. The initial beamline design was performed with 40 cm of graphite for simplicity.

The most obvious and also currently used target design is that of a cylinder and therefore the target radius is the most relevant parameter to consider. A cylinder with radius of 1 mm has been initially chosen as this fully accommodates the 2.4 mrad angle of the proton beam, including its varying transverse size throughout the focus. This is the same radius as the current T10 target and the smallest one that ensures the beam remains within the target throughout its length.

The choice of target radius is important as it affects the efficacy of the collimation system and therefore the experimental backgrounds. With an increased target radius, particles may be produced towards the edges of the target. After the first 'defining' collimation stage, any subsequent collimators must then avoid intercepting particles from the extremities of the target that pass through the first collimator aperture as this would create new background sources, in particular, K_s^0 regeneration. The combination of target radius and defining collimator aperture establishes a penumbra that cannot be intercepted. As the target radius increases so does the penumbra and therefore the ratio of background to useful beam at the experiment. The larger angle of 8 mrad proposed for HIKE Phase 3 would require a wider target rod that has not been considered in this baseline design [5].

However, at least one additional target head is foreseen in case the measured background rates during Phase 2 necessitate increasing the production angle. A clear choice is that the target head could be moved vertically only and would always be aligned to the axis of the beamline. A direct copy of the main target head would be used as an in-situ spare and a third target head would be one with a larger radius to accommodate an increased crossing angle as per the experiment requirements.

Inside the target shielding, a vertically moveable fixed aperture collimator will be placed immediately after the target to absorb large angle secondaries. Vertical movement would allow alignment to avoid intercepting the remaining high power proton beam if the crossing angle is varied. This could alternatively be made with a larger aperture and fixed in position from the beginning at the expense of a small increase in background from greater secondary particle leakage. A cylindrical, constant aperture in z was chosen with a radius of 7.5 mm, displaced 2 mm vertically downwards, with CuCrZr as the material. The material choice is not fixed and can be optimised in the technical design phase. This allows the desired secondary beam to pass and the remaining protons to pass towards the proton dump uninterrupted.

2.2 Proton Dump

Many high energy charge secondary pions and kaons emerge from the target. These ultimately decay and produce high energy muons that are highly penetrating and can be a

problematic background for the experiment as well as pose a radiation protection concern. Therefore, it is preferable to intercept these secondary pions as soon as possible where they will interact with matter and become lower energy before any decay happens. Ultimately, only some very low energy muons may escape that are both more easily deflected and shielded against.

Similarly, it is important to absorb the remaining protons passing through the target as far upstream as possible to give the greatest distance to shield against and deflect any products such as muons from the absorption of the protons.

It is proposed to use a vertically orientated MTR dipole magnet to deflect the remaining $400\,\mathrm{GeV}\,c^{-1}$ protons downwards immediately after the target housing. With its maximum current of 820 A, the magnet provides an integrated field of 7.38 T m. Following this, the new proton dump would be placed. An initial simplified design of 3.2 m of solid CuCrZr was used for simulations in this report, however, a further technical design would clearly need to refine this.

Simulations of the proton beam through the target in both FLUKA and BDSIM show that the spot size of the remaining protons at the front face of the proton dump would be approximately $\sigma_x = 2.0\,\mathrm{mm}$ and $\sigma_y = 1.21\,\mathrm{mm}$ and that it remains Gaussian. This is notably smaller than the beam size at the TAX for Phase 1, where the proton beam would be dumped ($\sigma_x = 4.7\,\mathrm{mm}$, $\sigma_y = 3.3\,\mathrm{mm}$), and initially this also appeared problematic due to the peak energy deposition. Defocussing the primary beam with quadrupoles requires too much distance after the dump and is not preferable in any case for the previously discussed design principle of removing high energy secondaries as soon as possible. One possibility is to increase the divergence of the proton beam by focussing more strongly onto the target. However, it would take a significant increase in divergence to increase the beam spot size at the proton dump, which is not compatible with the current P42 layout; in particular the available strength and aperture of the final focus quadrupoles. Additionally, given the overall small input beam spot size, the transverse size of the shower in the dump is dominated by the interaction in the first few centimetres of the CuCrZr of the dump. The results presented in this report use these original beam parameters as given in Table 1.

Initial thermo-mechanical simulations of the proton dump by SY-STI have shown that the maximum temperature reached (steady-state plus one immediate spill) in the proton dump would be less than that of the TAX and it would therefore not deform [7]. These simulations assumed 2.4×10^{13} protons per spill on the target (to give a margin of error), and also used the beam simulated from the upstream parameters given in Table 1. Furthermore, they included all secondary particles emerging from the target housing. This conclusion is reliant on the proton beam interacting with the target, which dilutes the beam and, given the one nuclear interaction length, only e^{-1} ($\sim 60\,\%$) of the proton beam survives.

The proposed proton dump does not need to move during operation but need only be aligned. Therefore, no support table is required as is typical with the movable TAX absorber and more material can be used below the beam axis to better absorb radiation. This is expected to have a positive impact on the required shielding in the floor of the cavern as compared to dumping the proton beam in the TAX, but this will need to be studied in detail in future.

An alternative considered for diluting the proton beam was an initial section of graphite in the proton dump, however, this would act like a secondary target in close proximity to

the neutral beamline and potentially could create high experimental backgrounds. Another alternative would be to allow the proton beam to pass through a wider aperture and use this initial dump only to absorb secondary radiation. Without magnetic sweeping, this would also be problematic as high energy forward-going pions can decay into high energy muons that are difficult to deflect sufficiently away from the experiment. It could still be regarded as a contingency in case problems with a dedicated proton dump arise.

The beamline design between the target and the Phase 1 TAX is relatively flexible given the constraints discussed above. A change here would not nominally have any knock-on effect for the collimator positions and their cleaning efficiency.

3 Acceptance and Collimation

3.1 Collimation Scheme

From the target, an acceptance cone of 0.4 mrad is requested within which a clean K_L^0 beam is desired, i.e. with as few other particles as possible. To define this acceptance, a collimation system is envisioned. It would consist of several collimators used in combination with dipole magnets placed downstream of them to sweep away any charged particles created in the collimators. The proposed scheme consists of an initial *defining* collimator that defines the acceptance, followed by two other collimators to clean any further background or scattered or secondary particles.

The optimal location of the collimators in a neutral beamline has been studied previously [4]. The defining collimator is optimally placed at 1/3 of the source to experiment length and the second collimator at a further 1/3 of the remaining distance. The optimum distance for the second collimator has a broad minimum so some flexibility is permitted. Specifically, the initial defining collimator is placed at 40 m (at its front face) from the centre of the target. The second collimator is placed at 66.6 m from the centre of the target and the third collimator is uniquely placed at the end of the beamline; i.e. its out-going face is 120 m from the centre of the target. The third collimator must also be instrumented (i.e. *active*) so it will tag any remaining experimental backgrounds.

3.2 Aperture and Shape

Each collimator is circular in aperture as there is axial symmetry for the desired neutral beam. Each collimator is shaped such that no surface faces both the target and the experiment as this would permit a particle to be scattered from the surface and reach the experiment directly. Therefore, each collimator is comprised of two cones; one incoming tapered cone; intersected with an outgoing divergent cone.

Practically, the required surface angles are very small and would be difficult to manufacture. To overcome this, one solution is a set of cylindrical inserts that would be placed into a larger cylindrical cut-out from a main block, approximating the cone-shape in steps. This design is currently used in various absorbers (TAX) in the North Area. The radii for each insert was quantised at 100 µm as this is a suitable manufacturing tolerance and is also the approximate 'skin-depth' for a 100 GeV c^{-1} kaon beam in tungsten [8]. The materials and dimensions of each collimator are given in Table 2. Each collimator is a square block

with a cylindrical cut out. The third collimator is an active collimator that is part of the experiment [1]. Instead of a tungsten insert it uses LYSO crystals that are transparent to optical wavelength light.

Although a narrow acceptance angle of 0.4 mrad is chosen for the experiment—corresponding to a radius of 4.8 cm at 120 m—a much larger 50 cm radius was chosen in consultation with the experiment where all backgrounds should be minimised as much as possible. This value was therefore used in the calculation of collimator surface angles with respect to the beamline axis.

Table 2: Collimator dimensions and materials.

#	Length (cm)	Outer Full Width (cm)	Outer Material	Insert Material	Insert Radius (mm)	Minimum Aperture Radius (mm)
1	120	20	CuCrZr	Tungsten	60.0	16.2
2	120	20	CuCrZr	Tungsten	60.0	28.1
3	80	100	CuCrZr	LYSO	100.0	62.2

An overview of the collimation system with general aperture is shown in Figure 2. A closer view of the first collimator is shown in Figure 3. This shows both the nominal angled surface desired and the quantised radii of inserts. An explanation of the collimator shapes is given below for each collimator.

- **Collimator #1** - the incoming cone angle is chosen such that a line from the start of the collimator, intercepting the narrowest radius at the aperture, when projected to the detector, is outside the nominal radius of the neutral beam at the interface plane (4.8 cm at $Z = 120$ m: 5 cm chosen to include a margin of error). This is so any reflected particle from the face cannot reach the detector. The outgoing cone is angled to match a line from the opposite side of the target passing the narrowest aperture. As such, no particle coming directly from the target can scatter on this outgoing conical surface.

- **Collimator #2** - the second collimator must not intercept particles that travel from the target that are reflected from the surface of the first collimator but remain intact as this would regenerate new backgrounds. Therefore its narrowest aperture lies outside the the acceptance cone and this larger 'penumbra' from collimator #1. This is shown in shaded pale blue in Figure 4. The incoming conical angle is chosen so that any particle reflecting from the surface goes outside the detector radius of 50 cm. The outgoing conical angle is chosen so that the surface is parallel to the maximum possible reflected particle from collimator #1.

- **Collimator #3** The final collimator is an active detector, serving to tag any particle passing outside of the nominal beam acceptance. Its aperture is chosen to be outside the nominal K_L^0 beam cone but largely covering the possible reflections from collimators along with an alignment tolerance. It is shown in Figure 5 and more fully described in section 3.3.

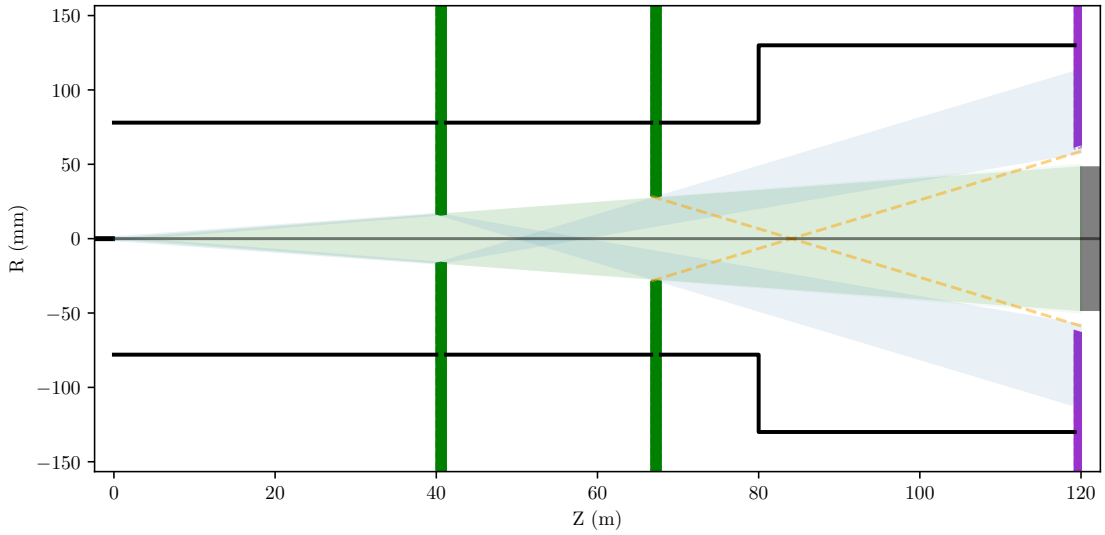

Figure 2: Overview of the collimation scheme with beam acceptance cone and possible reflection cones overlaid as a function of distance from the target (*left*) towards the experiment (*right*, grey box). The collimators are shown in dark green (#1, #2) and in purple (#3). Overlaid is the acceptance cone of the beam (pale green) and the possible reflection from the target towards the experiment (pale blue). The orange dotted lines show the possible closest reflection from the second collimator towards the experiment. The general vacuum aperture radius (ignoring vacuum windows and the air in the TAX) is shown as a black outline and the target (to scale) is the small black square at the left.

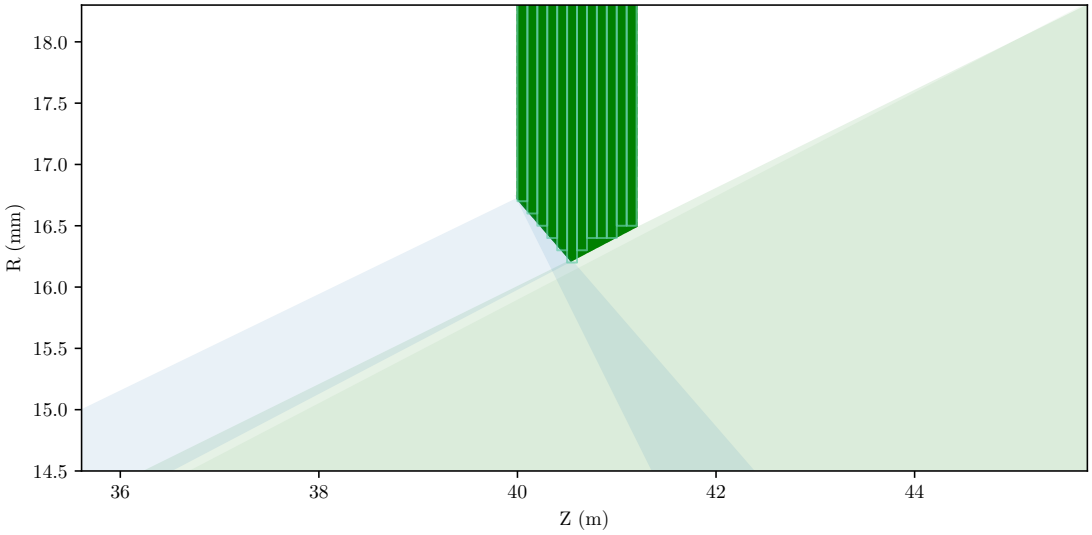

Figure 3: A closer cross section view of collimator #1 as a function of distance from the target. The nominal two-cone shape is shown in dark green with the quantised radii of inserts shown in light green overlaid. The large pale green shaded area shows the acceptance cone from the target including from the edge of the target. The pale blue area shows the possible illumination of the collimator front face from the target as well as the possible range of reflected angles. Only one side of the collimator is shown and the beam passes from left to right.

3.3 Active Final Collimator

The final collimator will be an active one that is part of the experiment. By intercepting any remaining halo or background particles it may indeed not fully absorb these particles or cause further secondaries to be produced. However, being an active detector, it tags these interactions, and such backgrounds can be vetoed by the experiment. The design of such an active collimator is described in [5]. A simplified design was included in this simulation of the beamline with a circular aperture and a similar set of four inserts. Each insert is made of a LYSO crystal with a surrounding of CuCrZr. A cross sectional view is shown in Figure 5.

3.4 Magnetic Sweeping

Being a neutral beamline of K_L^0 it is not possible to select by momentum or to magnetically guide or focus the desired particles. Magnetic fields are used only to dispose of any charged particles leaving only other neutral particles behind. An initial vertical dipole (MTR design) is used to both sweep the remaining primary protons downwards as well as deflect charged background including high energy pions as soon as they exit the target housing. This is crucial to avoid high energy on-axis muons being produced via decay that would create a large experimental background.

After each intercepting device, a magnet is placed to sweep away any charged particles produced. After the proton dump a horizontally oriented MTN magnet is used. After collimator #1 another MTN magnet (also horizontal) is used. After collimator #2, the pole

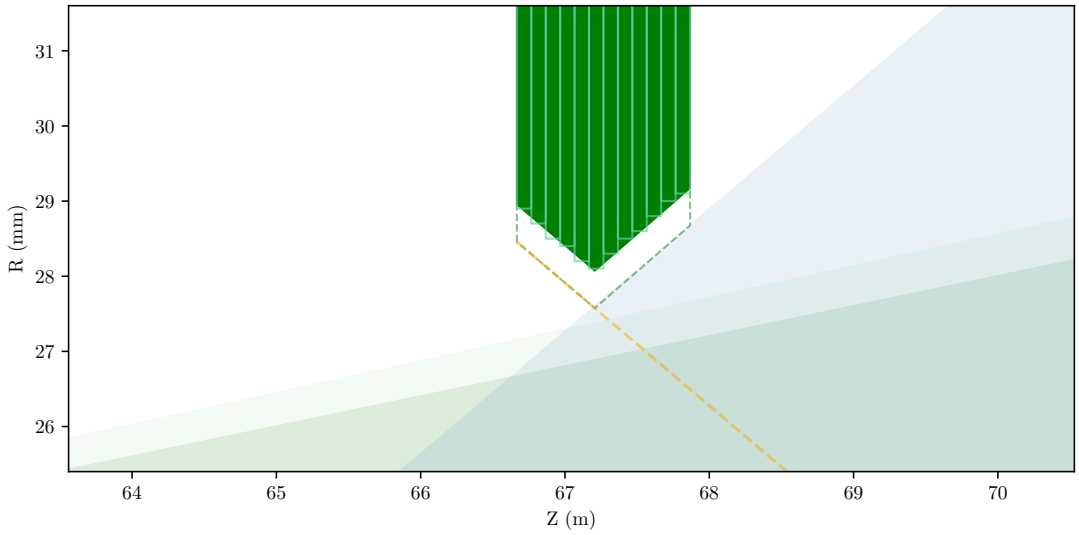

Figure 4: A closer cross section view of collimator #2 as a function of distance from the target. The nominal shape is shown in dark green with the quantised radii of inserts shown in light green overlaid. The pale green shaded area shows acceptance cone of the beam (lighter green from the extreme edge of the target). The pale blue area shows the possibly reflected beam from the first collimator. The dashed lines show the nominal perfect values. The collimator is retracted from this with an alignment tolerance to ensure no new background is created, marginally reducing its efficiency. The orange line shows the possible closest reflection angle from the surface (worst-case) towards the experiment.

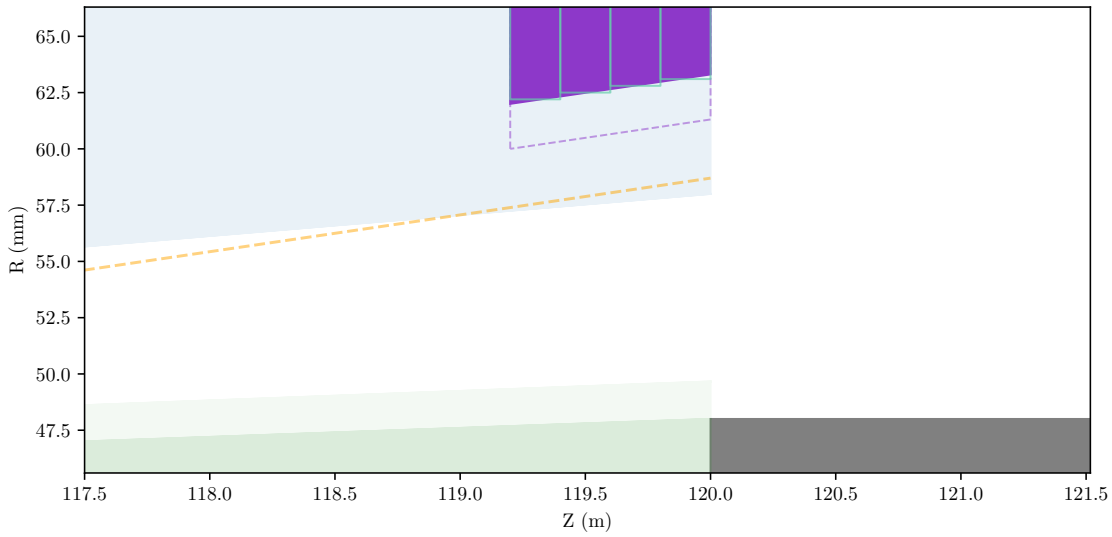

Figure 5: Closer view of collimator #3 as a function of distance from the target. The nominal K_L^0 acceptance cone is shown in pale green and lighter green for the extreme edge of the target. The pale blue area is the possibly reflected beam from collimator #1 originating from the target and the orange dotted line shows the minimum approach of any reflected particles from collimator #2. The collimator LYSO crystals are shown in purple with their quantised edges in light green overlaid. Only one half of the collimator is shown.

gap and therefore aperture in an MTN magnet is not sufficient so an MBPL magnet must be used. An MBPL magnet has a maximum bending power of 3.8 T m, which is weaker than the 7.8 T m of the MTN magnet, so two MBPL magnets are used. All magnets after the proton dump are orientated to give horizontal sweeping with a vertical magnetic field. This was found from studies for KLEVER [9], in combination with the vertical sweeping of the first dipole magnet before the proton dump, to give a minimal muon background due to the combined magnetic sweeping of the fields in the yokes of the magnets.

3.5 Phase 1 TAX

The current TAX design is an absorber consisting of 8 blocks of material movable in two groups of four. It is a crucial device for Phase 1 but unnecessary for Phase 2. However, it will be highly activated and cumbersome to remove after Phase 1 so it is proposed to leave it in place for Phase 2. Another hole that is not a defining aperture of the beam would be used and would remain in air without vacuum. Its length of approximately 4 m and remaining relatively narrow aperture makes it impractical to insert a vacuum pipe throughout it. Positively, it acts as further shielding for the experiment. The 4 m of air also has a negligible effect in the regeneration of K_s^0. The geometry model of the current K12 TAX was used but with the tungsten inserts from one hole removed from the model.

4 Gamma Converter

Of the neutral particles in the acceptance cone, γ and neutrons dominate. It is possible to reduce the number of γ without creating significant new background by introducing a thin plate of high-Z material where incident γ will create $e^{\pm}$ pairs. These charged particles can then be deflected by magnetic fields and absorbed. A high-Z material is preferred as the cross-section of pair production is proportional to $1/X_0$. However, too thick a converter would cause hadronic interactions with other particles in the beam and act like a new target, so only a thin piece of material can be used. Therefore, such a converter will not fully remove all gammas present but will reduce them significantly.

Traditionally, such a converter is ideally housed inside a larger absorber or shielding object such as the proton dump. This could be in vacuum, however, if it is inside the proton dump, it would complicate the design and its associated services. In the future, it is envisioned that a crystal may be used in place of an amorphous converter to possibly increase the efficiency of conversion whilst not adversely increasing the background generation. For such a device it would have to be rotatable to precisely align the crystal [1]. In this report, only an amorphous piece of material is considered. Tungsten of 4 mm length was the chosen thickness (along the direction of the beam) for a plate that is wide enough to cover the full acceptance cone, similar to the optimum found for the current K12 beam operation. Similarly, the plate was placed in the small air gap in the middle of the TAX absorber. The TAX would absorb any stray radiation created in the plate.

The spectra of γ before and after the converter plate when only considering those inside a radius of 10 cm is shown in Figure 6 from a Monte Carlo simulation in BDSIM (i.e. Geant4). Before the converter, and inside this radius, there are $3.0145 \pm 0.0011 \times 10^{12}$ γ per spill (assuming 2×10^{13} protons per spill on target). After the converter, there are $0.4035 \pm 0.0004 \times 10^{12}$ γ per spill, showing it significantly reduces their flux across all energies. Consequently there are more $e^{\pm}$ afterwards but these are swept away from the beamline axis by the subsequent magnets and do not reach the experiment.

5 Vacuum

Vacuum is essential in the beamline to minimise interactions and the creation of backgrounds. However, it is not practical nor entirely necessary to have all beamline elements under high vacuum conditions, in particular as HIKE Phase 2 has less severe constraints as compared to Phase 1. A typical level of 1×10^{-3} mbar as used in the upstream P42 beamline would be sufficient. The existing T10 target design is in air inside a shielding housing and the same was used for this simulation but with the new graphite target rod. At the exit of the target housing there is a vacuum window (200 µm of aluminium). The rest of the beamline is in vacuum with the exception of the TAX. The aperture chosen for the majority of the line is 156 mm inner diameter that is a commonly used standard in the North Area at CERN.

After the second collimator the cone of possibly scattered particles from the first collimator that leak through across the axis of the beamline becomes wider. The 156 mm aperture becomes restrictive and new backgrounds that would reach the detector inside the acceptance cone are created. This has been confirmed in Monte Carlo simulations where the origin of

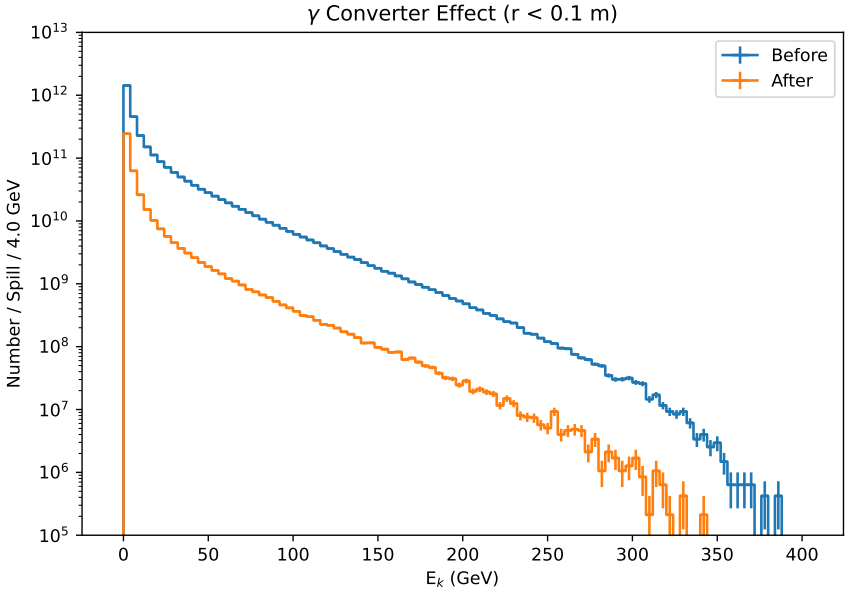

Figure 6: Comparison of the spectra of γ before and after the 4 mm tungsten converter plate situated in the middle of the TAX. The intensities are shown assuming 2×10^{13} protons per spill on target.

backgrounds reaching the experiment inside the acceptance cone originated from the beam pipe after the second collimator. Therefore, the aperture must be increased at approximately $z = 80$ m where a double width vacuum pipe (300 mm diameter) was chosen.

6 Shielding

As a baseline design, as little modification of the shielding is proposed as possible from the Phase 1 design. The beamline is also straight and the experiment remains in the same place between Phase 1 and Phase 2. Some modification may be required but this will be investigated in a later study for a technical design report. The design presented in this report is compatible with the existing shielding apart from a slight enlargement of the initial corridor close to the proton dump as discussed with HSE-RP. As already mentioned, the TAX will remain in place from Phase 1, which will increase shielding and reduce wider backgrounds to the experiment.

From previous studies [10], it was found that some backgrounds may pass by the side of the collimators and pass through between the poles and coils of the subsequent dipoles and reach the experiment if the same XCLD collimator design is used as in the NA48 case. Therefore, additional shielding is placed before collimator #1 and collimator #2. These would be iron blocks, 1 m long, that are sufficiently wide to cover the hole between the yoke of each dipole and the beam pipe. Collimator #2 along with this shielding and subsequent sweeping magnets is shown in Figure 7. As an alternative, new collimators could be specifically designed for this purpose.

For the purpose of the background simulations performed in this report, the compatibility

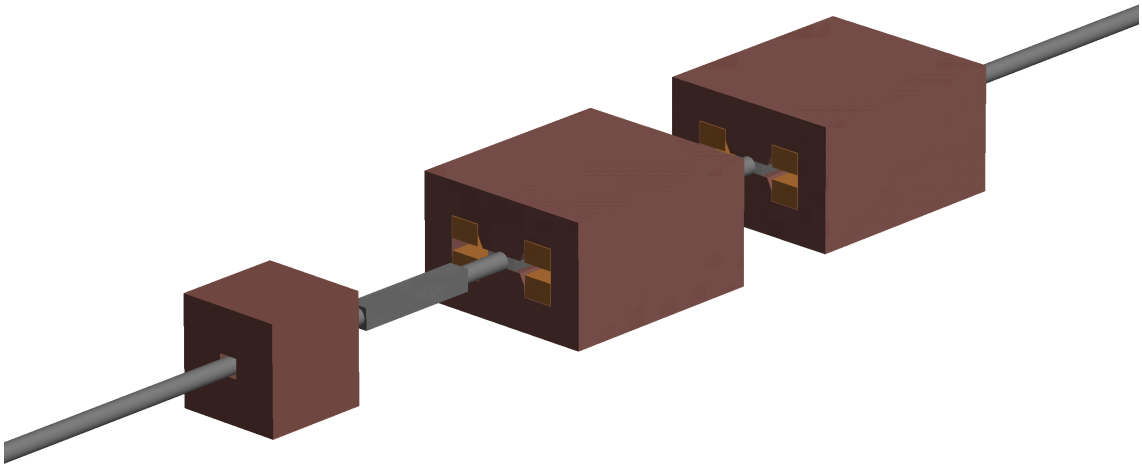

Figure 7: A 3D view of collimator #2 with shielding in front (*left*), the collimator itself in grey and two MBPL sweeping dipole magnets (*right*). The beam passes from left to right.

with the shielding was checked but the shielding itself was not included for the simulations as it did not affect the experimental backgrounds.

7 Simulated Beam and Background

Monte Carlo simulations were performed to evaluate the efficacy of the beamline design and the level of background the experiment can expect.

7.1 FLUKA and BDSIM

Both FLUKA [11] and BDSIM [12] codes were used to evaluate the beamline design. BDSIM, based on Geant4 [13, 14], was used for rapid development and trial of ideas as well as for understanding the history and origin of particles reaching the detector. Both models are ensured to be equivalent and the FLUKA model will be used in future for technical aspects such as the evaluating the radiation shielding, activation and muon fluxes outside the cavern. A view of the FLUKA model is shown in Figure 8 and a view of the BDSIM model is shown in Figure 9

7.2 BDSIM Model Setup

The BDSIM model uses externally created GDML files that contain accurate geometry for the majority of components and BDSIM-generated beam pipes are used to connect them. The geometry for each component was created using the pyg4ometry [15] Python library that allowed programmatic construction, e.g. collimator apertures calculated from equations of a line and quantised. Distributions were recorded at passive "sampler" planes placed at the incoming and outgoing faces of various elements. The final sampler after the third (*active*) collimator is defined as the interface plane where the beamline ends and the experiment

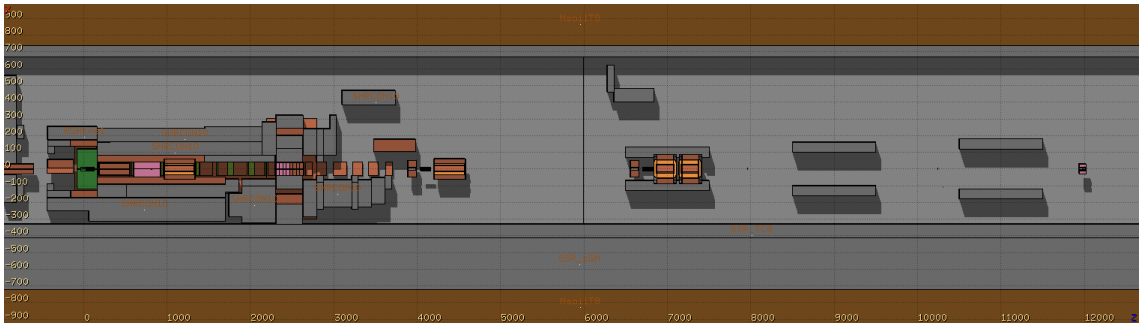

Figure 8: A 3D view of the HIKE Phase 2 FLUKA model as seen from above. The beam goes from left to right.

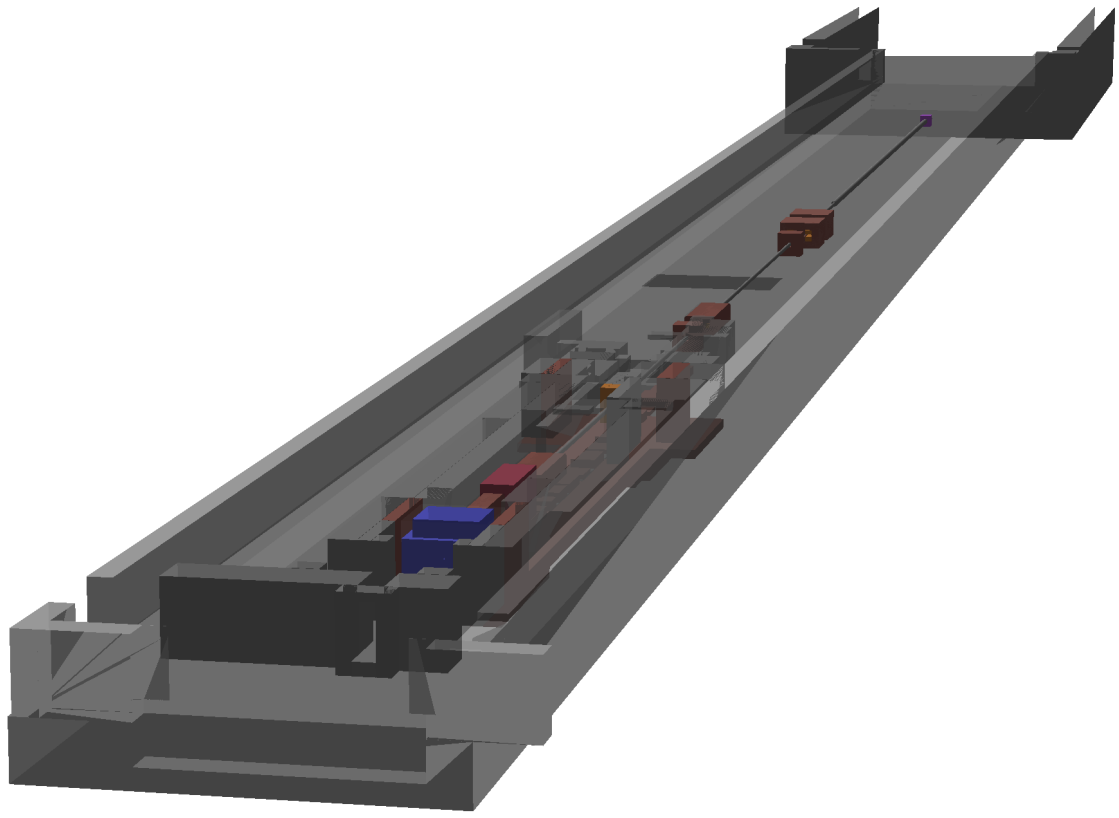

Figure 9: A 3D view of the HIKE Phase 2 BDSIM model with shielding included. The target housing is shown in blue and the proton dump in red. The beam goes from bottom left to top right. The final active collimator at $S = 120\,\mathrm{m}$ is shown in purple in the distance.

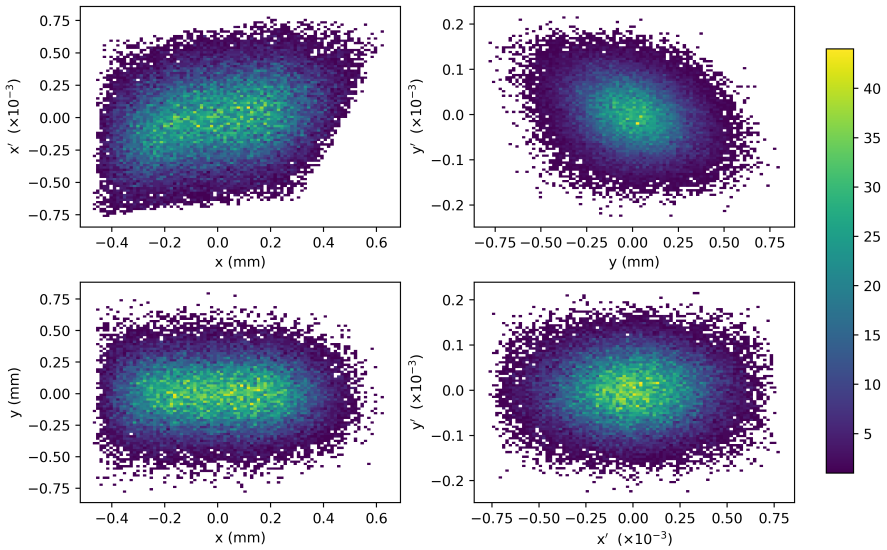

Figure 10: The initial 4D proton distribution used as shown at the centre of the target. The distribution is backtracked 0.7065 m before starting in the model.

starts. Additionally, select histories of tracks reaching the interface plane and their parent particles connecting them back to the primary proton were stored in BDSIM's output to understand the origin of backgrounds.

A realistic beam distribution supplied by SY-ABT was used as input [16]. It was generated by simulating the slow multi-turn extraction spill of the SPS as well as the magnetic splitting of the beam in the North Area. It has the equivalent proton beam parameters described in Table 1, but with a non-Gaussian shape due to the beam splitting after extraction from the SPS. In future, beam transport without magnetic splitting may be possible but the beam distribution would have the same size and divergence and the different here is negligible. The distribution is shown in Figure 10 at the centre of the target as supplied, but was back-tracked by 0.7065 m to the start of the target housing (and therefore the model) before being launched in the simulation. The supplied distribution comprises of 50000 particles, which is sufficient to represent a 4D distribution. Additionally, the 2.4 mrad angle and corresponding vertical offset were added to the distribution such that it arrives at the centre of the target with no offset.

BDSIM v1.7.4 was used, based on Geant4 10.7.2 including a patch that restores missing the proton-diffraction on atoms with baryon number > 10 (e.g. carbon in the target). 100 M events were simulated with a kinetic energy cut of 1 GeV. The Geant4 "FTFP_BERT" reference physics list was used along with lepto-nuclear interactions turned on providing the most accurate physics models available in Geant4, particularly for muon production. BDSIM's muon-splitting biasing was used with a splitting factor of 30 for muons produced with an initial kinetic energy $E_k > 3$ GeV. This muon-splitting operates on pions, kaons and positrons that produce muons in the relevant physics process. If a new secondary muon is observed when the physics process acts on the particle, the process is re-sampled N times and each muon weighted by $1/N$. Other secondaries are not split and their weight unaffected.

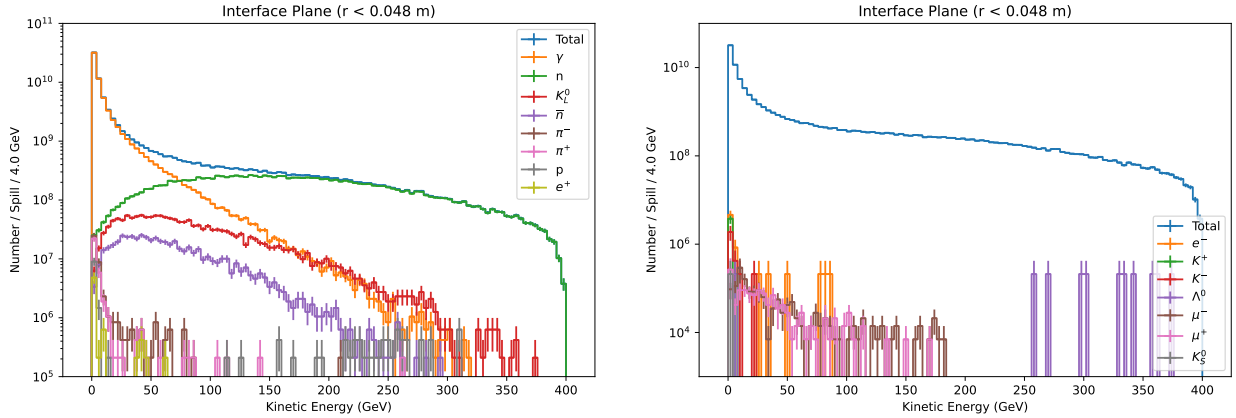

(a) Part 1 (b) Part 2

Figure 11: Spectra at $Z = 120\,\text{m}$ at interface plane after collimator #3 with a radial cut of 4.8 cm corresponding to the 0.4 mrad acceptance cone).

The statistical floor is therefore 1 in 1×10^8 where each event starts with 1 proton on target. The BDSIM software and environment used is available in perpetuity on the CVMFS file system [17] including the patch files for Geant4.

7.3 Beam Content

When assessing the efficacy of the beamline it is important to define different radii of interest from the beam axis. The nominal 0.4 mrad acceptance cone at $S = 120\,\text{m}$ gives a radius of 4.8 cm. Otherwise, a nominal 0.5 m radius can be considered for background purposes. Figure 11 shows the spectra at the interface place (i.e. after the third collimator) for a variety of radial cuts. The spectra are split into two figures for clarity and ordered by their integral.

As expected, there is a significant flux of neutrons and γ. Some charged particles remain but these are due to the decays of K_L^0 and Λ^0. Additionally, some small fraction of charged particles originate in the third collimator immediately before this interface plane, although few contribute inside this radial cut. It can be seen also that in Figure 11b, the muon distribution has a lower statistical floor than the Λ^0 due the splitting used.

The spectra of particles varies with different radial cuts. However, γ have almost no variation with radial cuts indicating that the vast majority of γ that reach the interface plane are within the 4.8 cm radial cut already shown. Similarly, for n and $\overline{n}$. The total number inside the 4.8 cm radial cut are summarised in Table 3. These results are in good agreement with previous studies of spectra for different collision angles and opening angles [10].

7.4 Muon Background

Apart from neutral backgrounds and backgrounds from the decay of neutral particles, the most relevant background is that of muons. These can be highly penetrating and of high

Table 3: Simulated particle fluxes inside a radius of 4.8 cm per spill where 2×10^{13} protons on target are assumed per spill with a simulation of 1×10^{8} protons on target.

Particle	Number / Spill	Number / Proton on Target
γ	$6.533 \pm 0.013 \times 10^{10}$	$3.226 \pm 0.007 \times 10^{-3}$
n	$1.531 \pm 0.006 \times 10^{10}$	$7.654 \pm 0.003 \times 10^{-4}$
K_L^0	$1.610 \pm 0.018 \times 10^{9}$	$8.050 \pm 0.092 \times 10^{-5}$
$\overline{n}$	$5.533 \pm 0.011 \times 10^{8}$	$2.767 \pm 0.054 \times 10^{-5}$
$\pi^{\pm}$	$7.893 \pm 0.067 \times 10^{7}$	$3.946 \pm 0.333 \times 10^{-6}$
p	$1.847 \pm 0.012 \times 10^{7}$	$9.236 \pm 0.996 \times 10^{-7}$
$e^{\pm}$	$1.343 \pm 0.025 \times 10^{7}$	$6.717 \pm 1.259 \times 10^{-7}$
$K^{\pm}$	$6.717 \pm 1.728 \times 10^{6}$	$3.359 \pm 0.864 \times 10^{-7}$
Λ^0	$2.309 \pm 0.700 \times 10^{6}$	$1.154 \pm 0.348 \times 10^{-7}$
μ^-	$1.508 \pm 0.216 \times 10^{6}$	$7.542 \pm 1.082 \times 10^{-8}$
μ^+	$1.232 \pm 0.237 \times 10^{6}$	$6.162 \pm 1.183 \times 10^{-8}$
K_S^0	$2.099 \pm 2.099 \times 10^{5}$	$1.050 \pm 1.050 \times 10^{-8}$

enough momentum that they are difficult to deflect sufficiently. Figure 12 shows the transverse distribution of muons at the interface plane at Z=120 m looking towards the target.

A crude mirror symmetry can be seen in the muon distribution due to the opposite deflection of the majority of muons by the upstream magnets depending on their charge. Analysis of the Monte Carlo data showed that the muons close to the axis come from the decays of particles also close to the axis that occur towards the end of the beamline. In Figure 13, the spectra as a function of different radial cuts at the interface plane is shown.

The overall low rate of muons close the central region shows effective handling of pions and muons upstream. In Figure 13, there are two large areas of muons in the transverse plane at the extremities, which are composed of muons between 50 GeV and 100 GeV but are deflected by over 1 m at the interface plane and miss the fiducial volume of the experiment. Were the first sweeping magnet further downstream after the target station, the spectrum of muons present would be of higher energy and closer to the axis of the beamline.

8 Summary and Further Investigation

A baseline conceptual design for a beamline to produce K_L^0 for HIKE Phase 2 has been presented. Several options for the handling of the primary proton beam and its absorption were considered but a baseline of a close-by proton dump to the T10 target was assumed for this study. A three-stage collimation system was designed to efficiently clean the beam as defined by a 0.4 mrad acceptance cone as well as minimise the regeneration of any further backgrounds in later collimation stages. The basic requirements for each component were laid out as well as the effect the choice of design parameters has on the neutral beam content and experimental backgrounds, which are crucial to making the proposed HIKE Phase 2 rare-decay measurements.

During a possible TDR phase in the case the HIKE experiment is approved, a more detailed design of the proton dump is required and this may consequently shift the subsequent

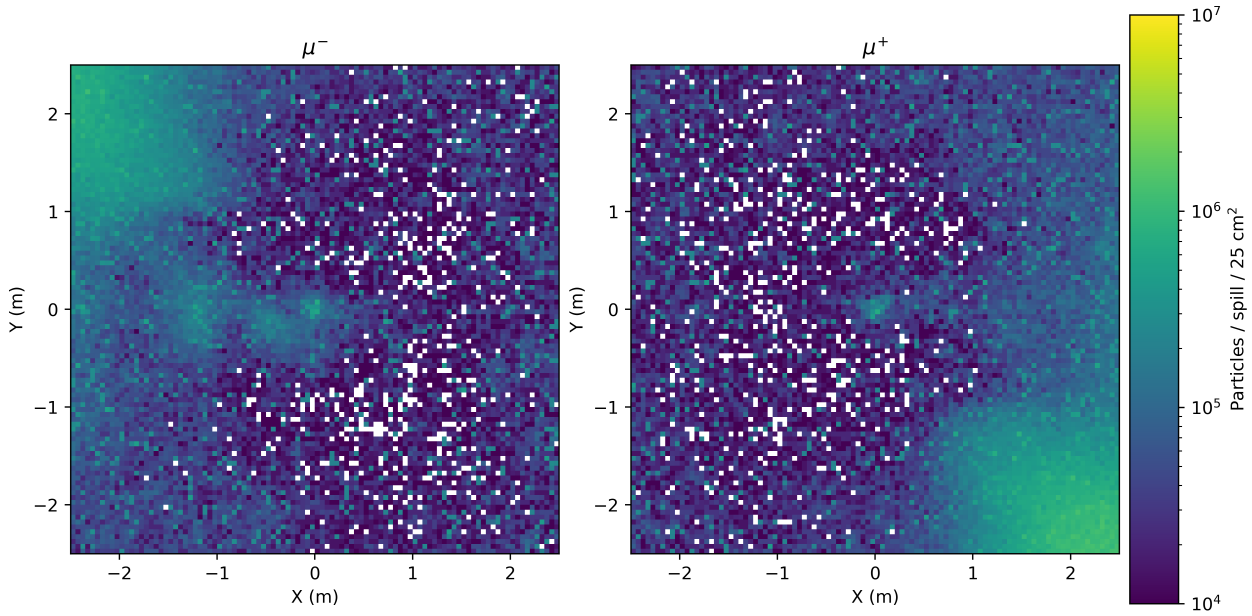

Figure 12: Muon distribution at the interface plane after collimator #3 for one spill assuming 2×10^{13} protons on target per spill.

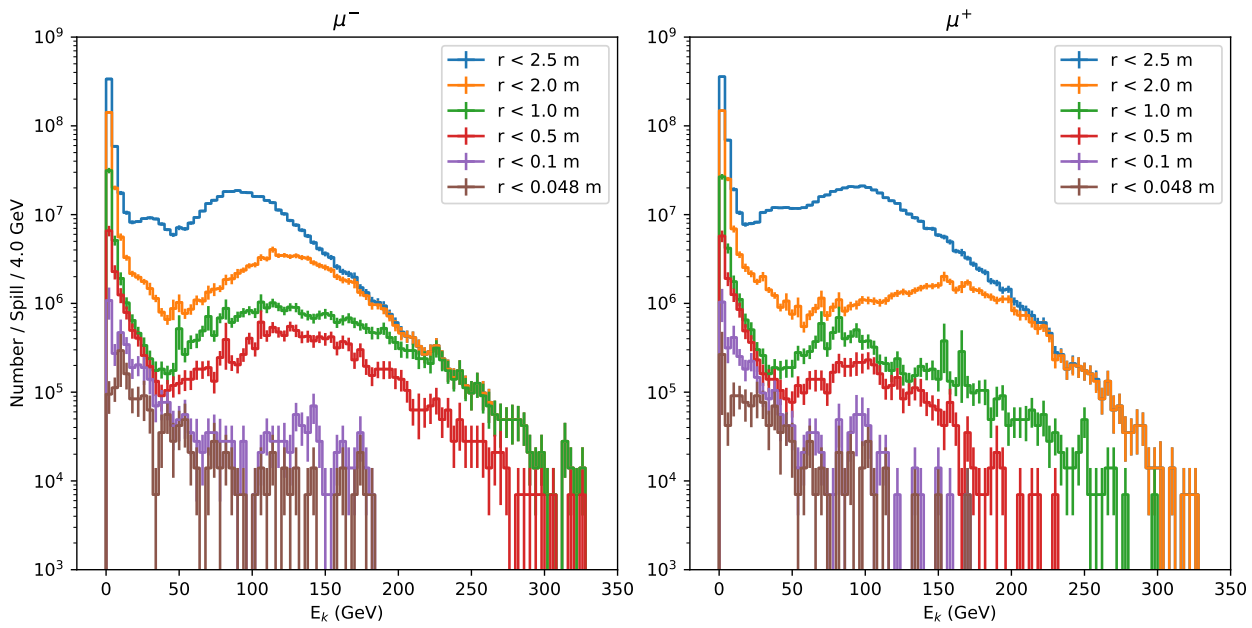

Figure 13: Muon spectra for various radial cuts at the interface plane at $Z = 120\,\mathrm{m}$ simulated for 2×10^{13} protons on target, i.e. for one spill.

horizontal sweeping magnet slightly. The radius of this proton dump aperture could be studied in future to optimise collimation of the secondary particles from the target whilst balancing thermal load on the material. The possible alignment of the TAX design with Phase 1 or indeed the evaluation of its complete removal from the beamline requires further study. Its removal and replacement with some shielding would permit continuous vacuum from the target to experiment. The overall shielding and integration concept need to be studied as the shielding in this study was used only for the purpose of a estimating detector backgrounds. In particular, this will require study of the muon flux and direction as well as the study of any required shielding that needs to be installed already in Phase 1 such as in the floor. It is foreseen that the compatibility of Phase 2 with Phase 1 would be considered in the TDR as some components would have to be installed before Phase 1.

Acknowledgements

We wish to thank N. Doble for interesting discussions, experience and ideas about how to design a neutral Kaon beam. Also, F. Metzger and F. Stummer for their aid in preparation of magnet geometry and field maps. We also would like to thank M. Fraser, F. Velotti and R. Ramjiawan (BE-ABT) for the input particle distributions.

References

[1] E. Cortina Gil et al., HIKE, High Intensity Kaon Experiments at the CERN SPS: Letter of Intent, CERN-SPSC-2022-031, SPSC-I-257, 11 2022.

[2] C Biino et al., The simultaneous long- and short-lived neutral kaon beams for experiment NA48, CERN-SL-98-033-EA, CERN-NA-48-NOTE-98-16, 1998.

[3] H. B. Greenlee, *Phys. Rev. D* **42** (1990) 3724.

[4] L. Gatignon, Design and Tuning of Secondary Beamlines in the CERN North and East Areas, CERN-ACC-NOTE-2020-0043, 2020.

[5] M. Moulson for the KLEVER Project, *J. Phys. Conf. Series* **1526** (2020) 012028.

[6] R. L. Workman and Others, *Prog. Theor. Exp. Phys.* **2022** (2022) 083C01.

[7] A. R Francia and R. F Ximenes, Discussion HIKE Phase 2 Proton Dump #3, https://indico.cern.ch/event/1339838/, 2023.

[8] G. L. D'Alessandro et al., *Nucl. Instrum. Meth. B* **512** (2022) 76.

[9] L. Gatignon et al., Report from the Conventional Beams Working Group to the Physics Beyond Collider Study and to the European Strategy for Particle Physics, CERN-PBC-REPORT-2018-002, CERN-PBC-REPORT-2022-002, 2022.

[10] Maarten Van Dijk and Marcel Rosenthal, Target studies for the proposed KLEVER experiment, CERN-ACC-NOTE-2018-0066, 2018.

[11] G. Battistoni et al., *Annals of Nuclear Energy* **82** (2015) 10.

[12] L.J. Nevay et al., *Comp. Phys. Comm.* **252** (2020) 107200.

[13] S. Agostinelli et al., *Nucl. Instrum. Meth. A* **A506** (2003) 250.

[14] J. Allison et al., *Nucl. Instrum. Meth. A* **835** (2016) 186 .

[15] S.D. Walker et al., *Comp. Phys. Comm.* **272** (2022) 108228.

[16] M. Fraser et al., Dedicated ECN3 optics particle distributions, EDMS 2767109, 2022.

[17] L. Nevay, BDSIM on CVMFS, `/cvmfs/beam-physics.cern.ch/bdsim/x86_64-centos7-gcc11-opt/bdsim-env-v1.7.5-g4v10.7.2.3-ftfp-boost.sh`, 2023, [Online; access 2023/10/01].

Appendices

A Beamline Element List

A list of key components is given in the table below.

Table 4: Summary of beamline elements for HIKE Phase 2 Beamline V1.3.

Name	Function	S Start (m)	S End (m)	L (m)
T10	Target Housing	-0.76	1.60	2.36
Begin Vacuum	Window	1.60	-	-
MTR 1	Dipole Vertical	1.91	5.51	3.60
Proton Dump	Dump	6.01	9.21	3.20
MTN 1	Dipole Horizontal	9.71	13.31	3.60
End Vacuum	Window	23.79	-	-
TAX	Existing Absorber	23.84	27.08	3.24
Begin Vacuum	Window	27.08	-	-
Shield 1	Surrounding	38.5	39.5	1.00
Collimator 1	Defining Collimator	40.0	41.2	1.20
MTN 2	Dipole Horizontal	41.7	45.3	3.60
Shield 2	Surrounding	65.16	66.16	1.00
Collimator 2	Cleaning Collimator	66.66	67.86	1.20
MBPL 1	Dipole Horizontal	68.36	70.36	2.00
MBPL 2	Dipole Horizontal	71.36	73.36	2.00
Aperture Transition	Wider Aperture	80.0	-	-
Collimator 3	Active Collimator	119.2	120.0	0.80
Interface	Interface Plane	120.0	-	-